

1 *Supplement of*

2 **Marine-Derived Water-Soluble Organic Nitrogen in Coastal Air: Influence of**
3 **Ocean Productivity on Atmospheric Nitrogen Cycling**

4 Jiao Tang^{1,2}, Shujie Hu^{3*}; Xiao Wang⁴; Jiaqi Wang⁵, Shaojun Lv²; Xiaofei Geng²;
5 Guangcai Zhong², Yangzhi Mo², Surat Bualert⁶, Jun Li², Shizhen Zhao^{2*}; Gan Zhang²

6

7 ¹ College of Marine Sciences, South China Agricultural University, Guangzhou 510642,
8 China

9 ² State Key Laboratory of Advanced Environmental Technology, Guangzhou Institute
10 of Geochemistry, Chinese Academy of Sciences, Guangzhou, 510640, China

11 ³ Chongqing Institute of Green and Intelligent Technology, Chinese Academy of
12 Sciences, Chongqing, 400714, China

13 ⁴ School of Resources and Environment, Henan Polytechnic University, Jiaozuo
14 454003, China

15 ⁵ School of Electrical and Information Engineering, Zhengzhou University, Zhengzhou,
16 450001, China

17 ⁶ Faculty of Environment, Kasetsart University, Bangkok, 10900, Thailand

18

19 **Contents of this file**

20 Number of Text: 3

21 Number of Tables: 5

22 Number of Figures: 10

23

24

25 **Text S1. PMF model**

26 Data Input

27 The data input includes concentrations and uncertainties of various types of chemicals
28 in 84 TSP samples. The types of chemicals include WSON, OC, EC, metal elements
29 (Ni, V, Pb, Cu, Zn, Mn, Fe), water-soluble ions (K^+ , Na^+ , Mg^{2+} , Ca^{2+} , NH_4^+ , Cl^- , SO_4^{2-} ,
30 NO_3^-), biomass burning tracers (levoglucosan, mannosan, galactosan), steranes,
31 hopanes, and SOA tracers (2-MGA, 2MGL, MBTCA, o/p-phthalic acid). The uncertainty
32 file provides species-specific parameters that EPA PMF 5.0 uses to calculate
33 uncertainties for each sample. If the concentration is less than or equal to the method
34 detection limit (MDL), the uncertainty (Unc) is calculated using a fixed fraction of the
35 MDL (1), and the concentration is replaced with half of the MDL.

$$36 \text{ Unc} = \frac{5}{6} \times \text{MDL} \quad (1)$$

37 If the concentration is higher than the MDL, the calculation is based on a user- provided
38 fraction of the concentration and MDL (Equation 2). Al element was set as bad,
39 resulting in solutions that didn't converge. Weak signals were found for species of
40 galactosan, mannosan, levoglucosan, hopanes and steranes, 2-MGA, and o-Phthalic
41 acid, which had a low signal-to-noise ratio ($S/N < 3$). Other species with an S/N greater
42 than 3 were set as strong.

$$43 \text{ Unc} = \sqrt{(\text{Error Fraction} \times \text{concentrations})^2 + (0.5 \times \text{MDL})^2} \quad (2)$$

44 Model run

45 The PMF model was executed using three to seven factors, 100 runs, and a random
46 starting point, resulting in converged solutions. Despite yielding the lowest $Q_{\text{robust}}/Q_{\text{true}}$
47 ratio (1.043, approaching unity), the six-factor solution exhibited mixing of the NH_4^+
48 and SO_4^{2-} with biomass burning tracers. This chemically implausible separation
49 rendered the six-factor interpretation problematic. Consequently, the seven-factor
50 solution was selected for source profile analysis as it provided physically meaningful
51 resolution.

52 *For WSON was set as the total variable:*

53 Uncertainty Estimation: To understand the uncertainty of the seven-factor solution, we
54 did a complementary analysis of displacement (DISP), BS, and bootstrapping with
55 displacement (BS-DISP). We used DISP intervals to include the effects of rotational
56 ambiguity, but not the effects of random errors in the data. BS intervals included the
57 effects of random errors and partially included the effects of rotational ambiguity. Finally,
58 BS-DISP intervals included the effects of both random errors and rotational ambiguity.
59 Tables S4–S5 show that the seven-factor solutions for WSON do not have significant

rotational ambiguity, and the base model and error estimates can be interpreted. With the absence of any swaps, dQ_{\max} provides confidence that these solutions are well constrained.

As shown in Figure S8, factor 1 was linked to high contribution of V, suggesting that it came from a shipping emission source (Celo *et al.*, 2015; Viana *et al.*, 2009). Factor 2 was characterized by high levels of NH_4^+ and SO_4^{2-} , which was a secondary sulfate source. Factor 3 (dust) shows a high contribution of Mn (69 %), Fe, Mg^{2+} , and Ca^{2+} . Factor 4 was identified as SOA source because it was associated with high loadings of 2-MGA, 2-MGL, MBTCA, and p-phthalic acid. Factor 5 was linked to biomass burning, with high loadings of galactosan, mannosan, and levoglucosan, NH_4^+ , NO_3^- , and p-phthalic acid also had high loading for this source, as reported in the source profiles of biomass burning (Li *et al.*, 2007). Factor 6 showed high loadings with Pb, Cu, and Zn and was identified as vehicle emissions and fossil fuel combustion. Factor 7 was associated with high levels of Na^+ , Cl^- , and Mg^{2+} , which was identified as sea spray aerosols via the bubble-busting processes (Facchini *et al.*, 2008).

Text S2. Potential Source Contribution Function (PSCF) Model

The PSCF model facilitates the identification of source region by partitioning the potential source domain into a grid matrix of $i \times j$, as detailed in our previous study (Geng *et al.*, 2020; Tang *et al.*, 2024). The PSCF analysis typically generates PSCF_{ij} values ranging from 0 to 1, with elevated PSCF_{ij} suggesting an increased likelihood that the ij_{th} cell being the source region. A notable constrain of PSCF-based methodologies is the necessity to establish a weighing function to designed to diminish the influences of cells with minimal residence time, a phenomenon often manifested as “trailing effects” (Petit *et al.*, 2017). To investigate the partitioning of aerosol sources and to ascertain the contributions of various aerosol emission sources and transportation mechanisms, we conducted a weighted Potential Source Contribution Function (WPSCF) analysis. Given that PSCF represents a conditional probability, the associated error escalates with increased distance between the grid and the sample points (Tiwari *et al.*, 2018). In this investigation, the experimental area was divided into a $0.25^\circ \times 0.25^\circ$ grid. The threshold for the computation of m_{ij} was established at the 75th percentile. To mitigate the impact of small n_{ij} values on PSCF, a weighting function was applied (Tiwari *et al.*, 2018):

$$w_{ij} = \begin{cases} 1.00 & n_{ij} > 80 \\ 0.70 & 20 < n_{ij} \leq 80 \\ 0.42 & 10 < n_{ij} \leq 20 \\ 0.05 & n_{ij} \leq 10 \end{cases} \quad (3)$$

Text S3 Predicting ALWC Using a Thermodynamic Model.

To predict the mass concentration of aerosol liquid water content (ALWC), we used a

thermodynamic model, ISORROPIA-II, <http://nenes.eas.gatech.edu/ISORROPIA/>, which calculates the ALW concentration with particle-phase concentrations of Na^+ , SO_2^- , NH_4^+ , NO_3^- , Cl^- , Ca^{2+} , K^+ , and Mg^{2+} , as well as meteorological conditions (RH and ambient temperature) as the input (Fountoukis and Nenes, 2007), which was described in our previous studies (Xu *et al.*, 2022). Briefly, the contributions of particle water associated with organic fractions to ALW were estimated by calculating the organic hygroscopicity parameter. ALW was calculated as the sum of water associated with individual aerosol chemical components (i.e., the sum of ions and lumped organics) based on the Zdanovskii–Stokes–Robinson (ZSR) relationship.

Table S1. The concentrations of TSP, OC, EC, WSON, $\text{NH}_4^+\text{-N}$, $\text{NO}_3^-\text{-N}$, and the ratio of OC/EC, WSON/WSON. In addition, the meteorological data, including relative humidity (RH), wind speed (WS), and temperature (Temp.) were also presented. Precipitation and radiation data are obtained based on historical reanalysis datasets from European Centre for Medium-Range Weather Forecasts (ECMWF). Cluster indicates the air masses that analyzed by HYSPLIT in Figures 1b and S1–S2.

Date	TSP ($\mu\text{g m}^{-3}$)	OC ($\mu\text{g m}^{-3}$)	EC ($\mu\text{g m}^{-3}$)	OC/EC	WSON ($\mu\text{gN m}^{-3}$)	$\text{NH}_4^+\text{-N}$ ($\mu\text{gN m}^{-3}$)	$\text{NO}_3^-\text{-N}$ ($\mu\text{gN m}^{-3}$)	RH (%)	WS (mph)	Temp. (°C)	Precipitation (mm)	Radiation (W m^{-2})	Cluster
2016/1/18	42	10	1.7	6.1	0.31	0.11	0.55	80	5.6	29	0.453	2845.62	1
2016/1/25	66	19	1.4	13	0.73	0.32	0.73	65	11	17	0.049	456.26	3
2016/2/1	97	18	2.4	7.7	1.2	0.34	1.6	75	4.3	30	0.264	4340.11	1
2016/2/8	161	38	2.8	14	1.1	2.2	2.7	43	7.8	21	0.000	8144.62	5
2016/2/15	88	15	1.9	8.0	1.3	0.28	1.1	76	5.8	30	0.115	3605.48	1
2016/2/22	60	11	1.8	5.9	0.89	0.58	1.3	74	6.7	29	0.017	3355.82	2
2016/2/29	118	23	1.9	12	1.3	1.1	0.69	48	5.0	29	0.000	4671.43	3
2016/3/4	101	13	1.6	8.1	1.3	0.40	0.75	71	6.8	30	0.004	4642.70	1
2016/3/8	47	8.7	1.3	6.7	0.35	0.51	0.98	74	9.2	30	0.094	4934.61	2
2016/3/10	37	9.7	1.6	6.0	0.50	0.34	0.58	78	7.5	30	0.000	4929.85	2
2016/3/14	33	8.0	1.3	6.2	0.49	0.10	0.45	73	7.8	31	0.000	5116.68	2
2016/3/16	40	9.9	1.4	7.3	0.41	0.22	0.56	69	9.7	31	0.005	5223.13	2
2016/3/18	59	10	1.4	7.5	0.71	0.52	0.50	74	9.4	31	0.001	5809.82	2
2016/3/20	51	8.0	1.0	7.9	0.60	0.48	0.44	74	11	31	0.000	5953.51	2
2016/3/22	80	13	1.6	8.1	0.91	0.75	0.34	74	9.0	31	0.000	7301.90	2
2016/3/24	111	15	1.7	8.9	0.65	1.26	0.55	64	7.3	32	0.000	6984.91	1
2016/3/26	54	11	1.2	9.3	0.80	0.71	0.78	59	8.3	30	0.184	3269.41	3

2016/3/28	111	24	2.1	12	1.2	2.10	2.7	68	7.1	29	0.016	2870.25	4
2016/3/30	57	11	1.4	7.6	0.84	0.54	0.94	77	6.2	30	1.276	3838.34	2
2016/4/1	43	8.3	1.3	6.2	0.54	0.39	0.82	71	8.7	31	0.278	4539.01	2
2016/4/3	18	6.1	0.83	7.3	0.57	0.35	0.39	68	8.7	31	0.012	4226.13	2
2016/4/5	28	6.9	1.1	6.2	0.64	0.13	0.39	69	8.8	32	0.168	5370.84	2
2016/4/7	35	8.7	1.2	7.2	0.57	0.31	0.32	72	10	32	0.064	3968.69	2
2016/4/9	25	5.4	0.95	5.7	0.53	0.09	0.24	67	10	32	0.012	5640.03	2
2016/4/13	63	8.7	1.3	6.6	0.59	1.8	0.28	55	9.8	33	0.000	6572.45	1
2016/4/15	37	7.1	0.95	7.5	0.41	1.1	0.12	65	9.8	33	0.224	5262.17	2
2016/4/17	32	7.9	0.16	49	0.27	1.1	0.10	71	9.7	33	0.544	5817.36	2
2016/4/19	26	6.2	1.1	5.9	0.41	0.57	0.12	68	9.7	32	0.448	5535.08	2
2016/4/21	34	6.6	0.91	7.2	0.57	0.07	0.41	63	9.9	32	0.372	4912.19	2
2016/4/23	38	8.4	0.99	8.5	0.92	0.08	0.35	65	10	33	0.311	5393.97	2
2016/4/25	40	9.8	1.1	8.6	0.98	0.35	0.26	69	9.7	33	0.218	5708.40	2
2016/4/27	47	11	1.2	8.5	1.2	0.53	0.44	69	9.7	33	0.438	4995.66	2
2016/4/29	29	7.1	1.0	7.1	0.84	0.36	0.16	72	9.1	33	0.152	4496.61	2
2016/5/1	20	5.4	0.96	5.6	0.84	0.23	0.20	74	6.4	30	0.580	4786.53	1
2016/5/3	23	5.7	1.3	4.3	0.77	0.31	0.18	63	8.5	33	0.443	5948.07	2
2016/5/5	21	5.4	0.91	5.9	0.88	0.09	BDL	66	7.9	33	0.003	5921.03	2
2016/5/9	20	3.7	0.63	5.9	0.66	0.06	0.20	61	10	34	0.058	4461.39	2
2016/5/11	36	8.7	1.0	8.5	1.1	0.19	0.34	66	9.5	34	0.647	5327.31	2
2016/5/15	44	11	1.1	9.5	1.1	0.50	0.53	73	7.7	31	2.188	3869.72	1
2016/5/17	41	9.9	1.1	8.8	1.2	0.67	0.64	76	6.8	30	2.089	2627.67	1
2016/5/19	36	7.7	1.1	7.0	0.93	0.17	0.29	66	7.9	32	0.792	3161.86	1
2016/5/21	25	5.8	0.94	6.2	0.92	0.02	0	65	9.3	32	1.402	2336.95	6

2016/5/23	39	7.1	0.93	7.6	0.98	0.39	0	63	10	31	12.116	2166.24	6
2016/5/25	39	8.1	1.4	5.7	0.69	0.11	0.31	58	11	32	1.066	1400.26	6
2016/5/27	39	6.6	1.0	6.6	0.78	0.16	0.39	62	8.3	32	1.198	2902.14	6
2016/5/29	46	6.0	0.88	6.8	0.89	0.23	0.52	61	8.8	32	2.901	902.48	1
2016/5/31	42	7.9	1.2	6.8	0.84	0.05	0.41	82	7.5	29	2.012	1927.43	1
2016/6/2	41	7.3	1.3	5.7	0.92	0.05	0.40	80	6.3	30	1.046	2302.63	2
2016/6/14	37	7.9	1.3	5.9	0.68	0.00	0.26	68	8.1	31	0.363	2907.11	6
2016/10/22	18	5.4	1.2	4.6	0.49	0.26	0.07	73	8.9	30	3.326	2077.57	6
2016/10/24	26	6.2	1.1	5.7	0.72	0.70	0.25	73	6.7	29	1.569	3366.86	1
2016/10/26	17	5.8	1.2	4.9	0.61	0.12	0.09	89	5.4	28	6.510	2059.29	4
2016/10/28	30	7.4	1.5	5.1	0.71	0.19	0.25	84	5.9	29	1.616	3684.34	4
2016/10/30	18	5.8	1.0	5.6	0.47	0.09	0.08	89	5.0	27	5.517	2707.15	5
2016/11/1	26	8.9	1.3	7.1	0.73	0.12	BDL	82	6.1	29	0.203	2615.73	3
2016/11/3	40	10	1.6	6.5	0.92	0.35	0.39	75	5.2	28	1.372	3752.32	3
2016/11/5	75	17	1.9	9.1	1.3	1.1	1.4	70	4.3	29	0.001	3672.66	4
2016/11/7	60	12	2.3	5.4	1.2	1.2	1.4	80	3.2	29	9.042	787.82	4
2016/11/9	43	10	1.7	6.1	1.2	0.62	0.98	89	5.3	28	6.884	317.76	4
2016/11/13	49	14	1.7	8.6	1.2	0.19	0.57	75	6.3	29	3.125	4701.36	5
2016/11/15	44	12	1.3	9.1	1.5	BDL	BDL	72	5.8	30	0.028	4410.31	5
2016/11/17	62	12	1.3	9.4	0.99	0.12	0.45	67	7.4	29	0.000	7075.15	5
2016/11/19	46	11	1.1	9.6	1.2	0.42	0.61	74	6.3	29	1.836	2255.39	4
2016/11/21	93	24	1.6	15	1.5	0.46	0.90	73	5.8	30	0.581	3279.00	4
2016/11/23	57	13	1.2	11	1.1	0.25	0.48	75	6.4	29	10.938	1452.02	4
2016/11/25	64	15	2.3	6.5	0.95	0.25	0.57	83	4.9	29	0.156	3046.12	5
2016/11/27	41	9.3	0.96	9.6	0.75	0.15	0.23	69	5.6	29	0.130	1766.73	5

2016/11/29	78	15	1.5	10	0.92	0.44	0.82	71	4.6	27	0.000	5736.78	5
2016/12/1	66	12	1.4	8.5	0.97	0.49	0.48	68	6.0	27	0.002	5181.22	5
2016/12/3	64	12	1.3	9.2	0.88	0.45	0.56	67	8.2	28	0.012	2908.52	5
2016/12/5	51	14	1.3	11	1.3	0.41	0.33	72	5.1	28	0.614	2746.71	5
2017/12/7	73	14	1.5	9.4	1.7	0.67	0.56	65	6.5	27	0.931	2198.62	5
2016/12/9	103	21	2.1	10	1.4	0.91	1.1	65	4.2	27	0.000	5908.49	5
2016/12/11	106	24	1.8	13	1.7	1.7	1.2	62	6.2	27	0.021	3175.09	4
2016/12/13	98	25	1.9	13	1.3	0.86	1.2	60	7.3	27	0.005	4615.21	4
2016/12/15	46	9.2	0.85	11	0.75	0.09	0.22	68	8.8	28	5.802	1251.42	3
2016/12/17	81	17	1.3	13	1.5	0.43	0.93	62	7.5	25	0.179	929.87	5
2016/12/20	124	29	2.0	15	2.1	0.75	2.1	65	5.8	29	0.003	3904.70	5
2016/12/27	50	13	0.92	14	1.0	0.17	0.40	58	5.9	29	0.000	5351.00	3
2017/1/3	57	12	1.3	9.8	1.1	0.20	0.54	70	7.6	27	0.114	2825.05	3
2017/1/7	110	25	2.0	12	2.3	0.59	1.3	71	7.0	28	2.041	330.58	4
2017/1/14	90	20	1.9	10	1.7	0.50	0.80	75	4.7	29	0.599	3377.36	5
2017/1/21	66	14	1.1	13	1.0	0.30	0.87	62	6.1	29	0.000	3822.33	3
2017/1/28	98	22	1.8	12	1.6	0.50	1.2	55	5.1	27	0.000	5900.06	4

109 BDL: below detection limits.

110

111

112 **Table S2.** The concentration of TSP, carbonaceous aerosol, WSON, WSIN, and
113 molecular markers in marine-, mixed-, and continental-influenced days.

	Marine (n = 36)		Mixed (n = 21)		Continental (n = 27)		All (n = 84)	
	Ave	SD	Ave	SD	Ave	SD	Ave	SD
TSP ($\mu\text{g m}^{-3}$)	42	21	54	24	73	34	55	30
OC ($\mu\text{g m}^{-3}$)	8.4	2.4	11	4.7	17	7.7	12	6.3
EC ($\mu\text{g m}^{-3}$)	1.2	0.32	1.4	0.48	1.6	0.40	1.4	0.43
WSOC ($\mu\text{g m}^{-3}$)	4.6	1.8	5.2	2.5	8.5	4.7	6.0	3.6
WSON ($\mu\text{gN m}^{-3}$)	0.72	0.25	1.0	0.34	1.2	0.43	0.95	0.40
NH_4^+ ($\mu\text{gN m}^{-3}$)	0.42	0.38	0.27	0.25	0.68	0.56	0.47	0.44
NO_3^- ($\mu\text{gN m}^{-3}$)	0.40	0.28	0.53	0.39	0.93	0.68	0.60	0.52
Na^+ ($\mu\text{g m}^{-3}$)	1.4	0.74	0.57	0.46	0.34	0.28	0.86	0.74
Cl^- ($\mu\text{g m}^{-3}$)	0.27	0.16	0.20	0.14	0.21	0.10	0.23	0.14
*nss- K^+	0.49	0.16	0.49	0.25	0.77	0.45	0.58	0.33
*nss- SO_4^{2-}	5.5	2.9	2.9	2.0	4.0	2.6	4.0	2.6
$\text{Na}^+/\Sigma\text{ions}$	0.11	0.040	0.060	0.038	0.028	0.023	0.028	0.023
OC/EC	8.1	7.2	8.4	2.4	10.1	3.0	8.9	5.2
WSOC/OC	0.54	0.11	0.44	0.08	0.49	0.08	0.50	0.10
WSON/WSOC	0.17	0.070	0.22	0.070	0.17	0.069	0.18	0.07
Molecular tracers (ng m^{-3})								
Levogluconan	70	54	140	112	337	282	174	207
Galactosan	2.3	1.4	4.9	3.6	11	8.2	5.6	6.17
Mannosan	5.8	3.8	9.2	6.3	17	12	10.3	9.29
Hopanes and steranes	1.2	0.4	1.3	0.7	1.3	0.7	1.3	0.60
2-MGA	3.2	1.5	5.0	2.6	6.6	4.1	4.8	3.2
2-MGL	36	22	29	17	38	23	35	21
MBTCA	11	7.2	31	22	29	12	22	17
o-Phthalic acid	7.9	4.4	4.1	3.4	7.5	7.3	6.8	5.5
p-Phthalic acid	10	7.9	31	25	43	26	26	25

114 nss-non sea salt

115

Table S3. The monthly averaged WSON concentration in the selected coastal cities that are impacted by marine air masses on a globe scale and the corresponding AEC (air mass exposure to Chl-a). The Chl-a concentration was from the MODIS-Aqua (EARTHDATA, <https://giovanni.gsfc.nasa.gov/giovanni/>).

Sites	Data	Monthly averaged WSON (nmol m ⁻³)	AEC (mg m ⁻³)	References
Keelung City	200607	27.2	0.136	Chen and Chen, (2010)
	200608	22.9	0.190	
South China Sea	200504	65	0.163	Shi <i>et al.</i> (2010)
Jiaozhou Bay, China	201507	190	0.860	Xing <i>et al.</i> (2018)
Hong Kong	201108	95	0.524	Ho <i>et al.</i> (2019)
	201109	95	0.319	
Hong Kong	201701	130.5	0.391	Leung <i>et al.</i> (2024)
	201703	114.7	0.306	
	201704	119.8	0.151	
	201705	117.0	0.230	
	201706	82.6	0.181	
	201707	114.8	0.250	
	201708	90.6	0.499	
	201709	93.3	0.445	
Eastern Mediterranean	201101	11.6	0.081	Tsagkaraki <i>et al.</i> (2021)
	201102	11.1	0.081	
	201104	9.45	0.118	
	201105	12.3	0.085	
	201106	22.2	0.071	
	201107	14.7	0.028	
	201108	16.4	0.082	
	201109	13.9	0.097	
	201110	8.12	0.073	
	201111	11.7	0.062	
	201112	9.71	0.081	
Okinawa Island	201006	34.6	0.068	Kunwar and Kawamura, (2014)
	201007	2.88	0.030	
	201008	2.88	0.035	
	201009	5.77	0.048	

	201010	4.32	0.141	
Barbados	200808	3.5	0.038	Zamora <i>et al.</i> (2011)
Huaniao island	201907	231.30	0.505	Tian <i>et al.</i> (2023)
	201908	211.56	0.474	
Sapporo	201006	6.56	0.159	Pavuluri <i>et al.</i> (2015)
	201007	4.63	0.135	
	201008	1.54	0.125	
Bangkok, Thailand	201601	36.96	0.197	This study
	201602	81.96	0.377	
	201603	52.03	0.199	
	201604	46.30	0.238	
	201605	63.93	0.311	
	201606	57.39	0.321	

120

121

122 **Table S4.** The mapping of bootstrap (BS) factors and Fpeak BS factors to base factors
 123 for seven-factor solutions. (Number of bootstrap runs: 100)

		Factor 1	Factor 2	Factor 3	Factor 4	Factor 5	Factor 6	Factor 7	Unmapped
BS Mapping	Factor 1	100	0	0	0	0	0	0	0
	Factor 2	0	91	0	3	2	4	0	0
	Factor 3	0	1	96	1	0	1	1	0
	Factor 4	0	1	0	99	0	0	0	0
	Factor 5	0	0	2	0	98	0	0	0
	Factor 6	0	0	0	1	0	99	0	0
	Factor 7	1	0	1	2	1	0	95	0
Fpeak BC Mapping (Fpeak value - 0.5)	Factor 1	100	0	0	0	0	0	0	0
	Factor 2	0	92	2	3	1	2	0	0
	Factor 3	0	0	96	3	1	0	0	0
	Factor 4	0	0	1	97	2	0	0	0
	Factor 5	0	0	1	2	96	1	0	0
	Factor 6	0	0	0	2	0	98	0	0
	Factor 7	1	1	1	3	0	1	93	0

124

125

126

127

128 **Table S5.** Displacement (DISP) diagnostics of seven-factor solutions. Bootstrapping
 129 with displacement (BS-DISP) diagnostics of seven-factor solutions.

Constrained DISP Diagnostics:							
Error Code:	0						
%dQ:	-0.016758291						
Swaps by Factor:	0	0	0	0	0	0	0
Constrained BS-DISP Diagnostics:							
# of Cases:	81						
%dQ:	-0.106123702						
Swaps by Factor:	0	5	1	2	4	3	3

130

131

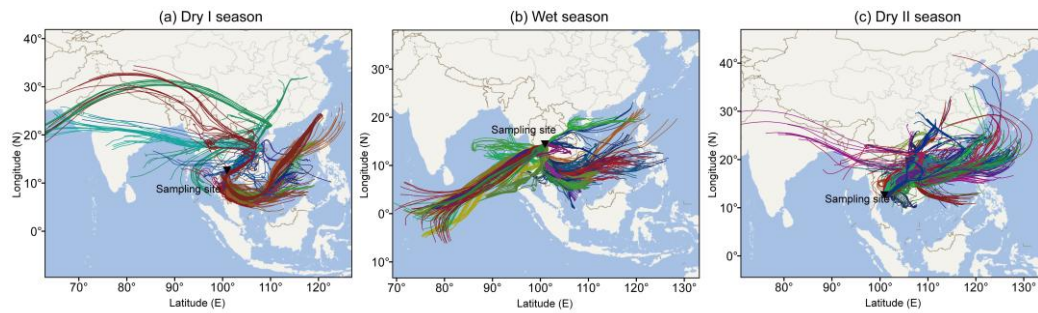


Figure S1. The 120 h back air-mass trajectories at Bangkok, from Thailand, in the Dry I (a), Wet (b), and Dry II seasons (c). The air mass trajectories were analyzed using the HYSPLIT model. The map was created using ArcGIS software, while the base map was acquired from the National Platform for Common Geospatial Information Services (www.webmap.cn).

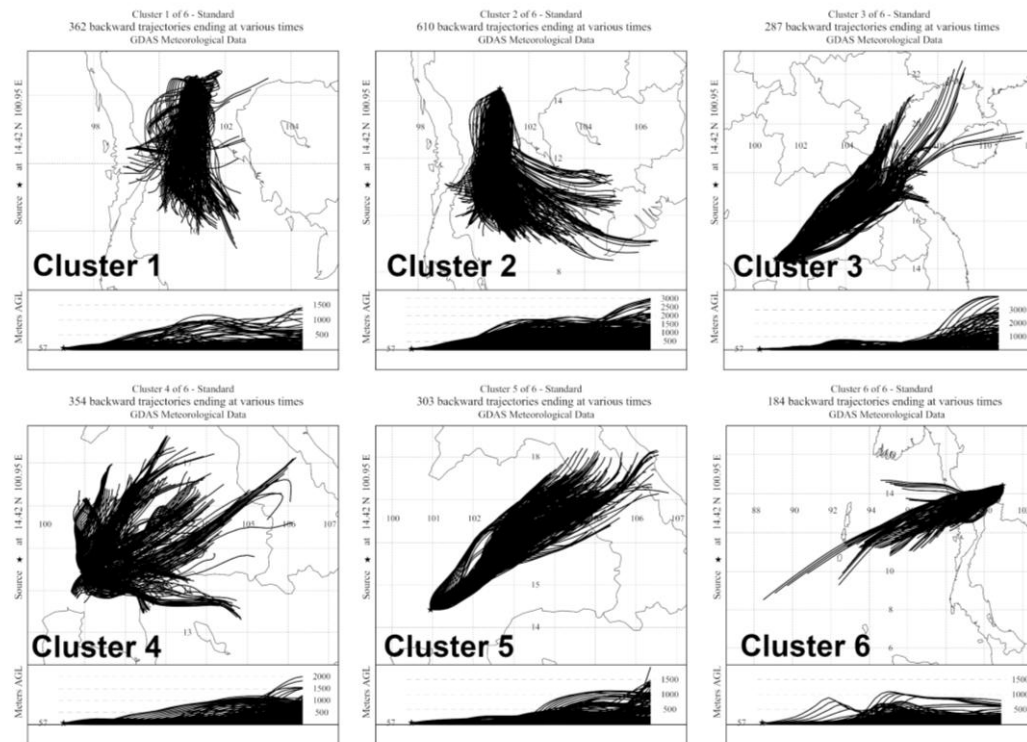


Figure S2. The 120 h back air-mass trajectories at Bangkok, from Thailand, during January, 2016 to January, 2017. The backward trajectories were clustered into six groups. The air mass trajectories were analyzed using the HYSPLIT model. According to the air cluster, cluster 1, 2, and 6 classified as marine air masses, and cluster 3, 4, and 5 were classified as continental air masses.

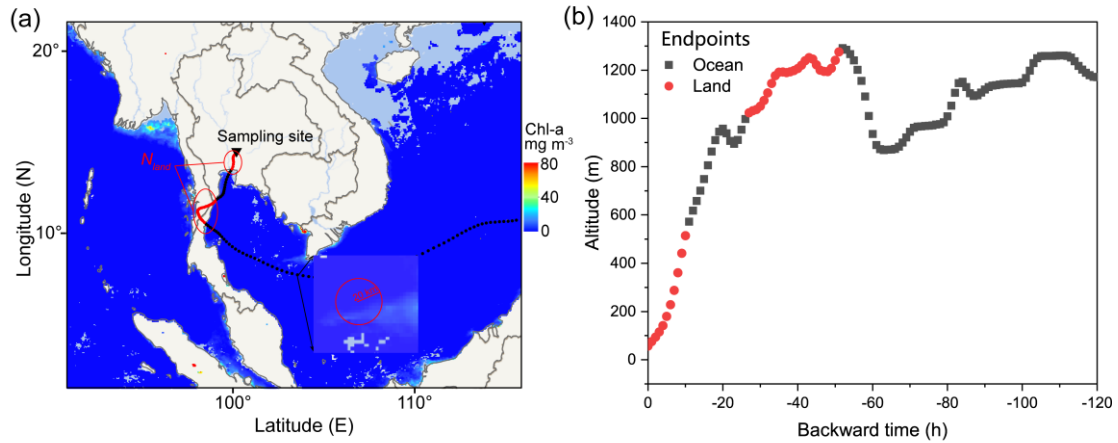


Figure S3. Schematic diagram of the calculations of (a) R_{land} and AEC, and (b) altitude of each air mass endpoints (b) using 120-hour trajectories. The red points refer to the endpoints along trajectories located over the land. This 20 km radius was representative of the area used as the search radius to compute the mean Chl-a concentration at the air mass endpoints.

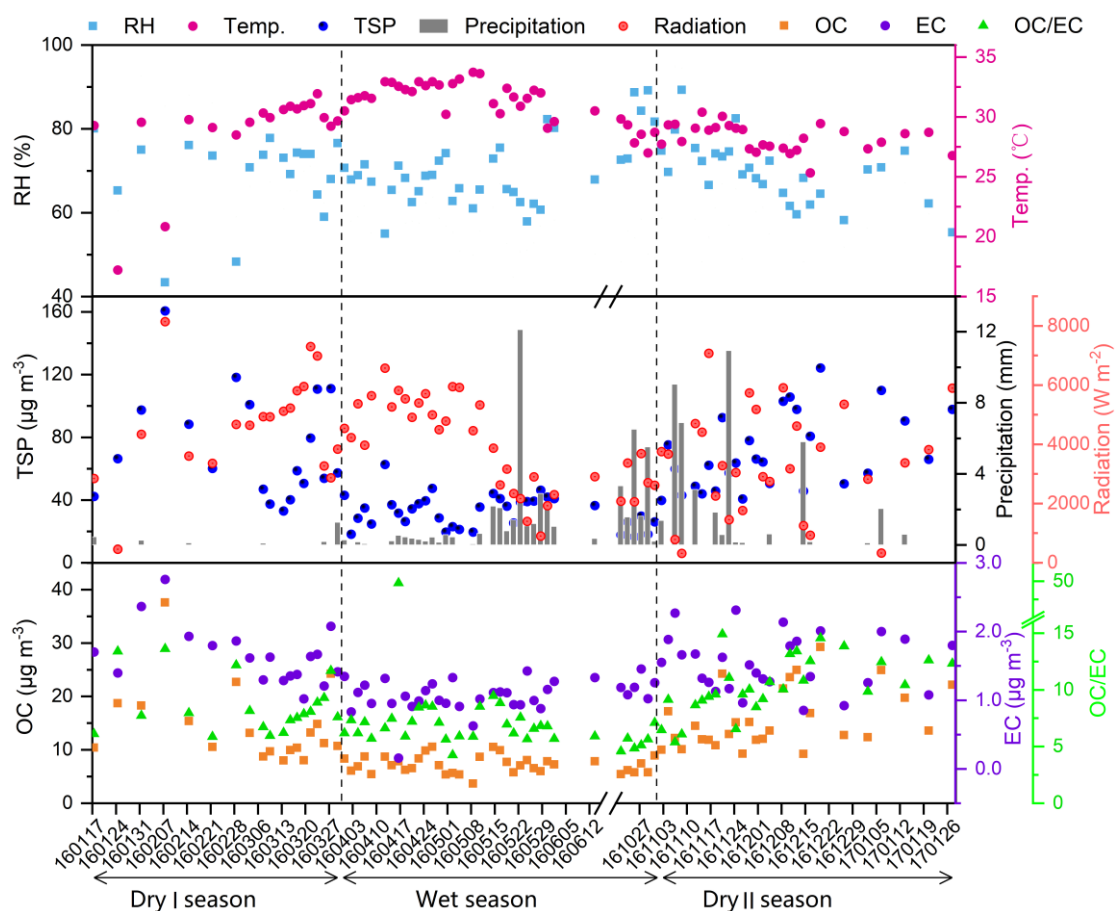


Figure S4. Meteorological data including relative humidity (RH), temperature (Temp.), precipitation, and radiation, along with time-series of TSP, OC, EC, and the ratio of OC/EC.

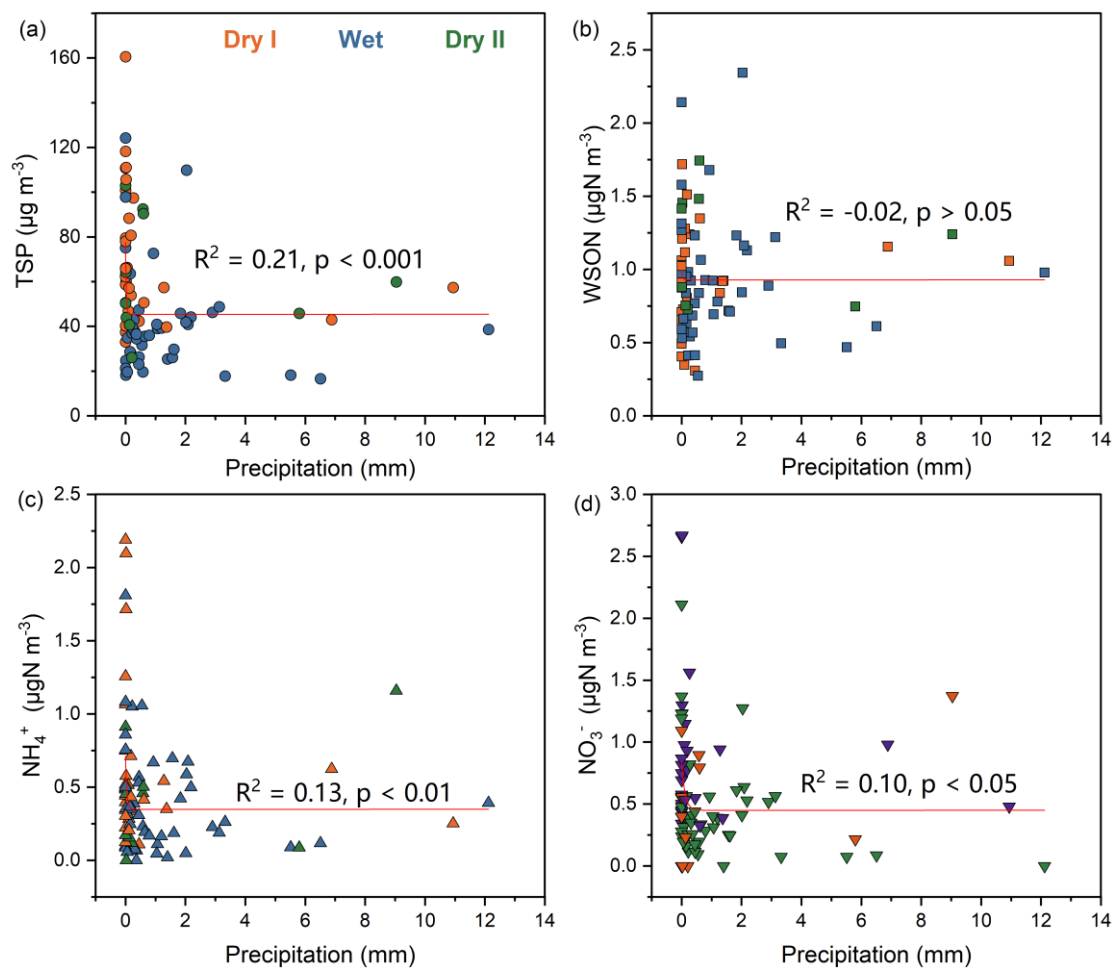


Figure S5. Exponential curve between TSP (a), WSON (b), WSIN (c, d) and precipitation.

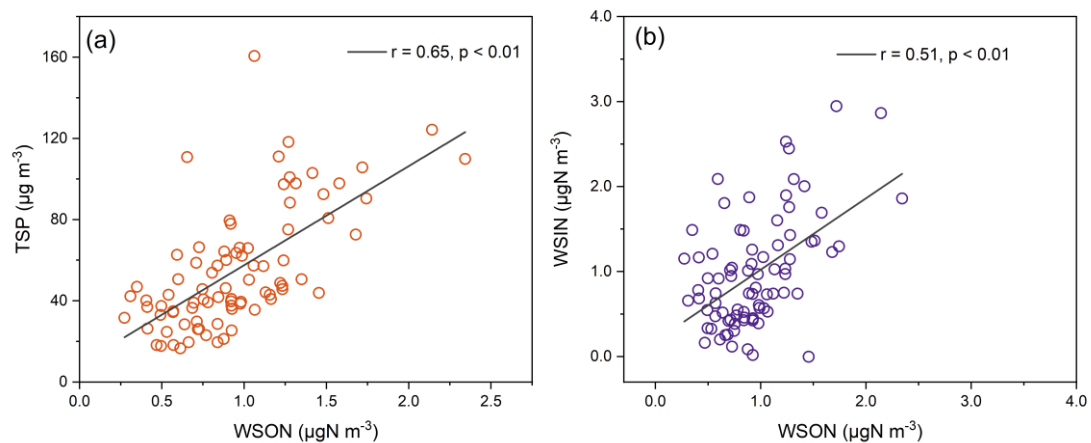


Figure S6. Linear relations of WSON to WSIN (sum of NO_3^- -N and NH_4^+ -N).

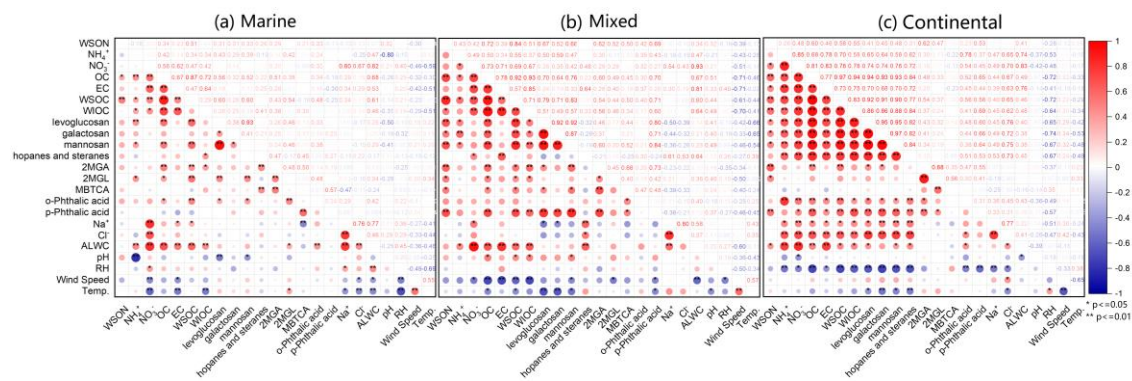


Figure S7. The correlation hotpots in marine- (a), mixed- (b), and continental-influenced days (c).

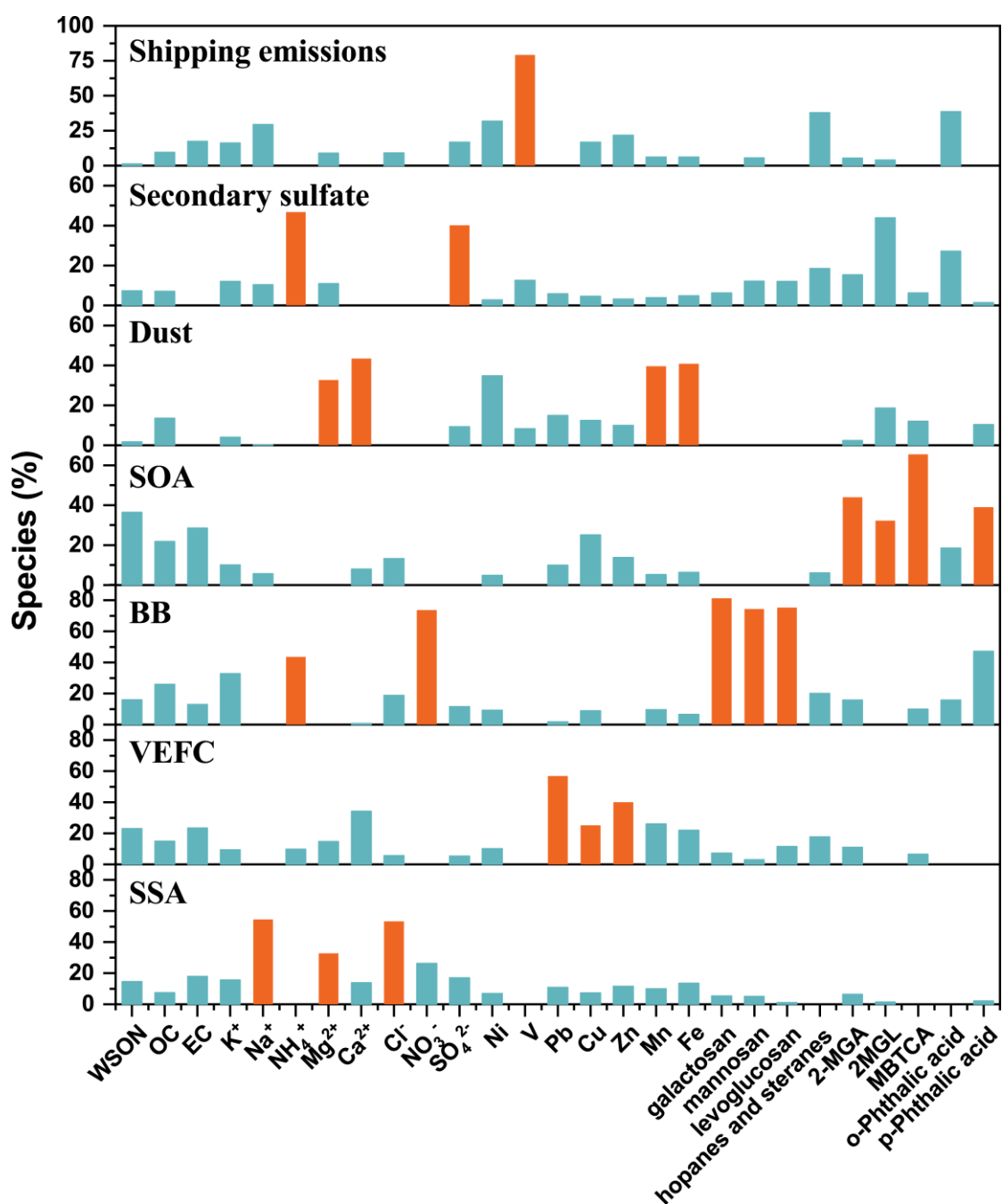


Figure S8. Seven factor profiles derived from the PMF solution. The percentage of chemical species in each factor is shown.

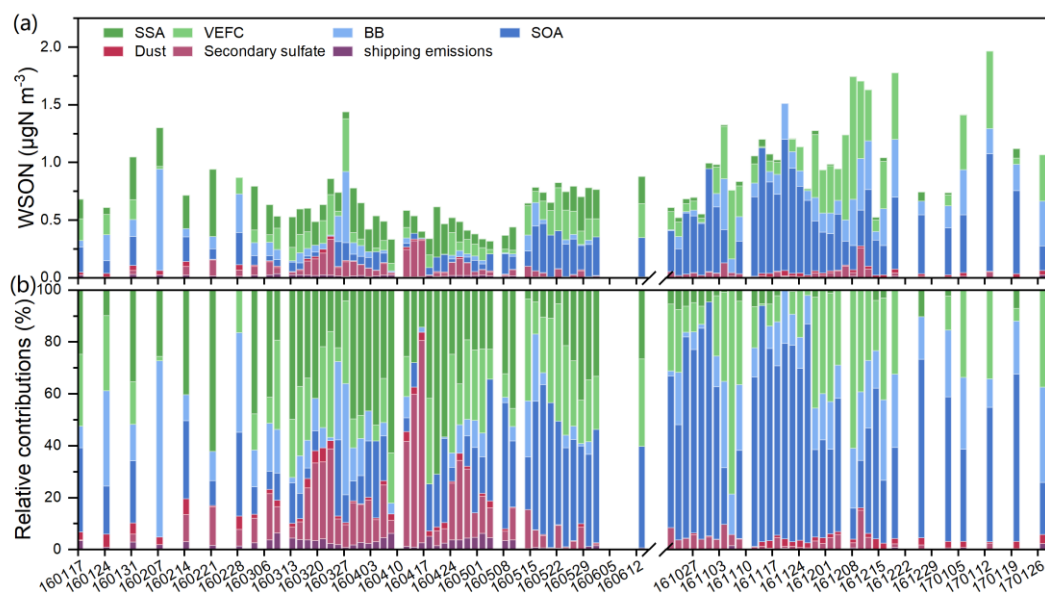


Figure S9. The time series of seven PMF source factor and the relative contributions to WSON (a, b).

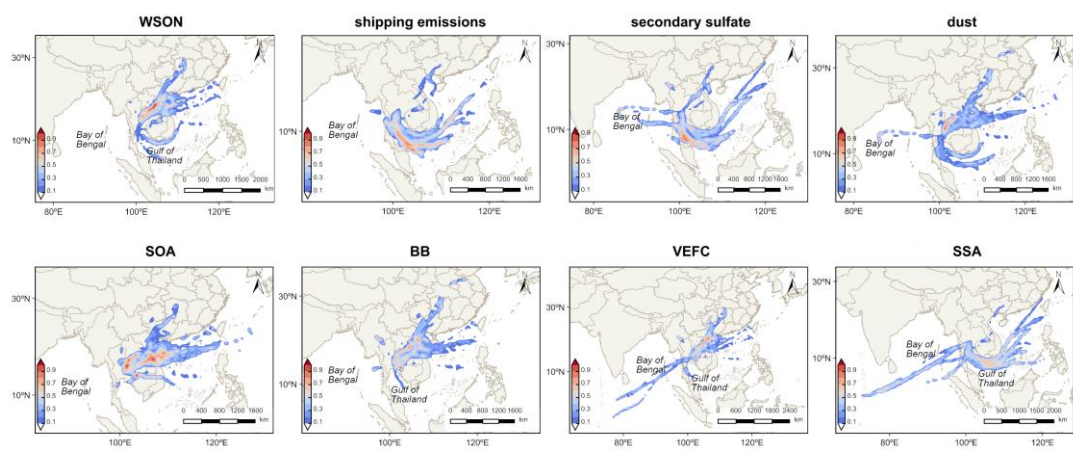


Figure S10. PSCF results of WSON and the seven-factor derived WSON resolved by PMF model. Threshold values were set as the 75th percentile of the corresponding values. The 120-hr backward air mass trajectory was analyzed using the HYSPLIT model.

References:

- Celo, V., E. Dabek-Zlotorzynska, and M. McCurdy (2015), Chemical Characterization of Exhaust Emissions from Selected Canadian Marine Vessels: The Case of Trace Metals and Lanthanoids, *Environ. Sci. Technol.*, 49(8), 5220-5226, <https://doi.org/10.1021/acs.est.5b00127>.
- Chen, H.-Y., and L.-D. Chen (2010), Occurrence of water soluble organic nitrogen in aerosols at a coastal area, *J. Atmos. Chem.*, 65(1), 49-71, <https://doi.org/10.1007/s10874-010-9181-y>.
- Facchini, M. C., et al. (2008), Primary submicron marine aerosol dominated by insoluble organic colloids and aggregates, *Geophys. Res. Lett.*, 35(17), <https://doi.org/10.1029/2008GL034210>.
- Fountoukis, C., and A. Nenes (2007), ISORROPIA II: a computationally efficient thermodynamic equilibrium model for K^+ - Ca^{2+} - Mg^{2+} - NH_4^+ - Na^+ - SO_4^{2-} - NO_3^- - Cl^- - H_2O aerosols, *Atmos. Chem. Phys.*, 7(17), 4639-4659, <https://doi.org/10.5194/acp-7-4639-2007>.
- Geng, X., Y. Mo, J. Li, G. Zhong, J. Tang, H. Jiang, X. Ding, R. N. Malik, and G. Zhang (2020), Source apportionment of water-soluble brown carbon in aerosols over the northern South China Sea: Influence from land outflow, SOA formation and marine emission, *Atmos. Environ.*, 229, 117484, <https://doi.org/10.1016/j.atmosenv.2020.117484>.
- Ho, S. S. H., L. Li, L. Qu, J. Cao, K. H. Lui, X. Niu, S.-C. Lee, and K. F. Ho (2019), Seasonal behavior of water-soluble organic nitrogen in fine particulate matter (PM_{2.5}) at urban coastal environments in Hong Kong, *Air Qual. Atmos. Health*, 12(4), 389-399, <https://doi.org/10.1007/s11869-018-0654-5>.
- Kunwar, B., and K. Kawamura (2014), One-year observations of carbonaceous and nitrogenous components and major ions in the aerosols from subtropical Okinawa Island, an outflow region of Asian dusts, *Atmos. Chem. Phys.*, 14(4), 1819-1836, <https://doi.org/10.5194/acp-14-1819-2014>.
- Leung, C. W., X. Wang, and D. Hu (2024), Characteristics and source apportionment of water-soluble organic nitrogen (WSO_N) in PM_{2.5} in Hong Kong: With focus on amines, urea, and nitroaromatic compounds, *J. Hazard. Mater.*, 469, 133899, <https://doi.org/10.1016/j.jhazmat.2024.133899>.
- Li, X. G., S. X. Wang, L. Duan, J. Hao, C. Li, Y. S. Chen, and L. Yang (2007), Particulate and trace gas emissions from open burning of wheat straw and corn stover in China, *Environ. Sci. Technol.*, 41(17), 6052-6058, <https://doi.org/10.1021/es0705137>.

219 Pavuluri, C. M., K. Kawamura, and P. Q. Fu (2015), Atmospheric chemistry of
 220 nitrogenous aerosols in northeastern Asia: biological sources and secondary formation,
 221 *Atmos. Chem. Phys.*, 15(17), 9883-9896, <https://doi.org/10.5194/acp-15-9883-2015>.
 222 Petit, J. E., O. Favez, A. Albinet, and F. Canonaco (2017), A user-friendly tool for
 223 comprehensive evaluation of the geographical origins of atmospheric pollution: Wind
 224 and trajectory analyses, *Environ. Modell. Softw.*, 88, 183-187,
 225 <https://doi.org/10.1016/j.envsoft.2016.11.022>.
 226 Shi, J., H. Gao, J. Qi, J. Zhang, and X. Yao (2010), Sources, compositions, and
 227 distributions of water-soluble organic nitrogen in aerosols over the China Sea, *J.*
 228 *Geophys. Res.-Atmos.*, 115(D17), <https://doi.org/10.1029/2009JD013238>.
 229 Tang, J., et al. (2024), Long-Emission-Wavelength Humic-Like Component (L-HULIS)
 230 as a Secondary Source Tracer of Brown Carbon in the Atmosphere, *J. Geophys. Res.-*
 231 *Atmos.*, 129(5), e2023JD040144, <https://doi.org/10.1029/2023JD040144>.
 232 Tian, M., et al. (2023), Seasonal source identification and formation processes of
 233 marine particulate water soluble organic nitrogen over an offshore island in the East
 234 China Sea, *Sci. Total Environ.*, 863, 160895,
 235 <https://doi.org/10.1016/j.scitotenv.2022.160895>.
 236 Tiwari, S., D. Kaskaoutis, V. K. Soni, S. Dev Attri, and A. K. Singh (2018), Aerosol
 237 columnar characteristics and their heterogeneous nature over Varanasi, in the central
 238 Ganges valley, *Environ Sci Pollut Res Int*, 25(25), 24726-24745,
 239 <https://doi.org/10.1007/s11356-018-2502-4>.
 240 Tsagkaraki, M., C. Theodosi, G. Grivas, E. Vargiakaki, J. Sciare, C. Savvides, and N.
 241 Mihalopoulos (2021), Spatiotemporal variability and sources of aerosol water-soluble
 242 organic nitrogen (WSON), in the Eastern Mediterranean, *Atmos. Environ.*, 246, 118144,
 243 <https://doi.org/10.1016/j.atmosenv.2020.118144>.
 244 Viana, M., F. Amato, A. Alastuey, X. Querol, T. Moreno, S. García Dos Santos, M. D.
 245 Herce, and R. Fernández-Patier (2009), Chemical Tracers of Particulate Emissions
 246 from Commercial Shipping, *Environ. Sci. Technol.*, 43(19), 7472-7477,
 247 <https://doi.org/10.1021/es901558t>.
 248 Xing, J., J. Song, H. Yuan, Q. Wang, X. Li, N. Li, L. Duan, and B. Qu (2018), Water-
 249 soluble nitrogen and phosphorus in aerosols and dry deposition in Jiaozhou Bay, North
 250 China: Deposition velocities, origins and biogeochemical implications, *Atmos. Res.*,
 251 207, 90-99, <https://doi.org/10.1016/j.atmosres.2018.03.001>.
 252 Xu, B., et al. (2022), Large contribution of fossil-derived components to aqueous
 253 secondary organic aerosols in China, *Nat. Commun.*, 13(1), 5115,
 254 <https://doi.org/10.1038/s41467-022-32863-3>.

255 Zamora, L. M., J. M. Prospero, and D. A. Hansell (2011), Organic nitrogen in aerosols
256 and precipitation at Barbados and Miami: Implications regarding sources, transport and
257 deposition to the western subtropical North Atlantic, *J. Geophys. Res.-Atmos.*,
258 116(D20), <https://doi.org/10.1029/2011JD015660>.

259